

Exceeding the Landau Superflow Speed Limit with Topological Bogoliubov Fermi Surfaces

S. Autti,^{1,2} J.T. Mäkinen,^{1,3,4} J. Rysti,¹ G.E. Volovik,^{1,5} V.V. Zavjalov,^{1,2} and V.B. Eltsov^{1,*}

¹*Department of Applied Physics, Aalto University, POB 15100, FI-00076 AALTO, Finland*

²*Department of Physics, Lancaster University, Lancaster LA1 4YB, UK*

³*Department of Physics, Yale University, New Haven, Connecticut, 06520, USA*

⁴*Yale Quantum Institute, Yale University, New Haven, Connecticut, 06520, USA*

⁵*L.D. Landau Institute for Theoretical Physics, Moscow, Russia*

A common property of topological systems is the appearance of topologically protected zero-energy excitations. In a superconductor or superfluid such states violate the Landau criterion for dissipationless flow. We check experimentally whether stable superflow is nevertheless possible in the polar phase of p-wave superfluid ^3He , which features a Dirac node line in the energy spectrum of Bogoliubov quasiparticles. The fluid is driven by rotation of the whole cryostat, and superflow breakdown is seen as the appearance of single- or half-quantum vortices. Vortices are detected using the relaxation rate of a Bose-Einstein condensate of magnons, created within the fluid. The superflow in the polar phase is found to be stable up to a finite critical velocity ≈ 0.2 cm/s, despite the zero value of the Landau critical velocity. This stability is provided by the accumulation of the flow-induced quasiparticles into pockets in the momentum space, bounded by Bogoliubov Fermi surfaces. In the polar phase this surface has non-trivial topology which includes two pseudo-Weyl points. Vortices forming above the critical velocity are strongly pinned in the confining matrix, used to stabilize the polar phase, and hence stable macroscopic superflow can be maintained even when the external drive is brought to zero.

I. INTRODUCTION

There are two factors which support stability of supercurrent in superfluids and superconductors: topological stability and the Landau criterion. Topological stability protects quantized circulation of the supercurrent in a ring geometry. The Landau criterion protects the supercurrent against decays by the creation of quasiparticles when the flow velocity is below the Landau critical velocity $v_{\text{cL}} = \min[E(\mathbf{p})/p]$, where $E(\mathbf{p})$ is the energy spectrum of quasiparticles with momentum \mathbf{p} . In Fermi superfluids and superconductors $v_{\text{cL}} \approx \Delta/p_F$, where Δ is the gap in the energy spectrum of Bogoliubov quasiparticles and p_F is the Fermi momentum. In topological systems, appearance of sub-gap (in particular, zero-energy) states or presence of nodes in the energy gap is ubiquitous. How does this affect stability of supercurrent in topological superconductors and superfluids?

Remarkably, in the topological superfluid phases of ^3He , supercurrent may persist when one of those constraints, or even both are not obeyed. Topological protection is absent in the chiral superfluid $^3\text{He-A}$, where the circulation is topologically unstable towards a phase slip with the formation of skyrmions [1, 2]. However contrary to the statement in Ref. [2], the superflow persists up to velocity $v \sim 0.1$ cm/sec [3]. Moreover, this velocity exceeds the Landau critical velocity, which is actually zero in $^3\text{He-A}$ due to presence of two point nodes [$E(\mathbf{p}) = 0$] in the energy spectrum.

There are two reasons why supercurrent in $^3\text{He-A}$ remains stable under the violation of the Landau crite-

ri- on and in the absence of topological protection. On one hand, the absence of topological stability does not exclude local stability of superflow, which is supported by different factors such as anisotropy of the superfluid density, effects of boundaries, applied magnetic field or spin-orbit interaction. Under experimental conditions, the superflow is locally stable until the threshold is reached, at which the instability develops with formation of skyrmions [3].

On the other hand, $^3\text{He-A}$ is a Fermi superfluid. In Fermi superfluids, superflows exceeding the Landau critical velocity do not necessarily lead to the destruction of superfluidity [4]. In the super-Landau superflow some Bogoliubov quasiparticle states acquire negative energy. Fermionic quasiparticles start to occupy those energy levels forming a Fermi surface. Such Fermi surface, which emerges in a superfluid or in a superconductor is called the Bogoliubov Fermi surface (BFS). In superfluid ^3He and cuprate superconductors [5–8] it appears due to supercurrent, but in systems with a multiband structure of the energy spectrum or in systems with broken time-reversal symmetry it may exist even in the absence of supercurrent [9–15].

Appearance of the BFS gives rise to a non-zero density of states at zero energy and thus to a non-zero normal component density ρ_n at $T = 0$. When all the negative states are occupied, the equilibrium value of $\rho_n(T = 0)$ is reached, and the non-dissipative superflow is restored, though with smaller superfluid density, $\rho_s(T = 0) = \rho - \rho_n(T = 0)$. The superflow above the Landau critical velocity remains stable until some other critical velocity v_c is reached. This can be either the velocity at which $\rho_n(T = 0) = \rho$ and thus the superfluid density $\rho_s = \rho - \rho_n$ vanishes, or the critical velocity at which quantized

* vladimir.eltsov@aalto.fi

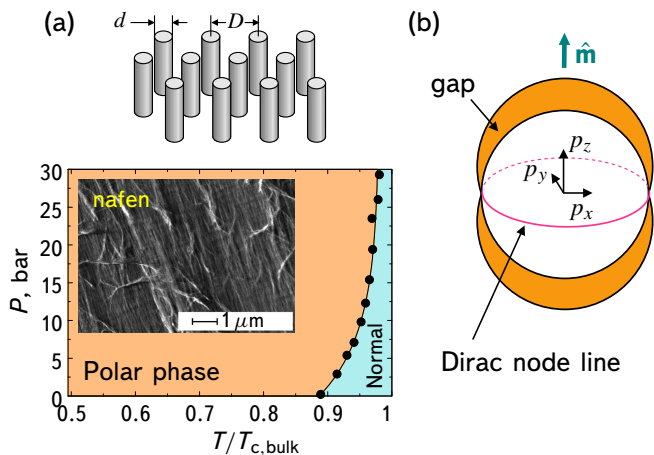


FIG. 1. The polar phase engineered with nanostructured confinement. (a) When ${}^3\text{He}$ is confined between parallel solid strands with appropriate dimensions, the polar phase appears below T_c . It was realized using commercial nafen material with $d \approx 9$ nm and $D \approx 35$ nm [25]. When D is increased to 50 nm, the polar-distorted A and B phases are also found on the phase diagram at lower temperatures. (b) In the stationary polar phase, the energy spectrum of Bogoliubov quasiparticles includes a Dirac node line in the plane perpendicular to strands.

vortices or skyrmions are created. Such super-Landau superflow has been recently reported in the fully gapped superfluid ${}^3\text{He-B}$ [16], see also [17].

The superfluid phases of ${}^3\text{He}$ [18] serve as a rich repository of exotic quantum phenomena in condensed matter and relativistic quantum vacua [4, 19]. Properties of these topological superfluids can be tuned in a wide range using nanoscale confinement [20–23]. Recently a new phase of ${}^3\text{He}$, the time reversal symmetric polar phase, Fig. 1, has been engineered using such confinement [24–26]. Here we report the violation of the Landau criterion in the polar phase and discuss topology of the resulting Bogoliubov Fermi surface. In the polar phase the Landau critical velocity is zero due to presence of the node line in the quasiparticle energy spectrum. Nevertheless, we find that the supercurrent remains stable to essentially higher velocity, up to 0.24 cm/sec. At higher velocities it becomes unstable towards the creation of quantized vortices. The appearance of vortices is detected based on the increased relaxation rate of a Bose-Einstein condensate of magnon quasiparticles [27, 28]. Furthermore, we find that the forming vortices are strongly pinned to the strands of the confining matrix, which results in dynamics similar to vortex dynamics in superconductors. Vortices, created by rotation, remain in the sample for days after the rotation is stopped (as long as the temperature remains low enough). Thus, we are able to maintain long-living superflow exceeding the Landau critical velocity even in a stationary sample. These observed features of vortex dynamics in the polar phase are supported by numerical simulations.

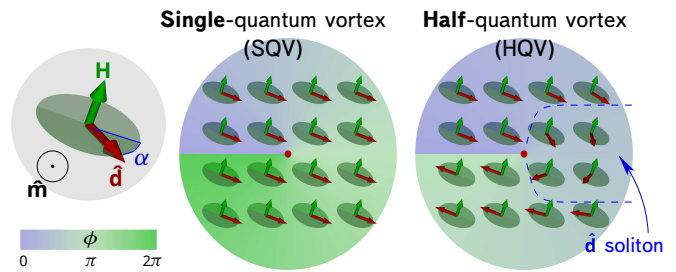


FIG. 2. Types of quantized vortices in the polar phase. The order parameter phase ϕ (background color) winds by 2π around a single-quantum vortex, and by π around a half-quantum vortex. To keep the order parameter single-valued, vector $\hat{\mathbf{d}}$ (red arrows) also rotates around the HQV core, so that $\hat{\mathbf{d}} \rightarrow -\hat{\mathbf{d}}$ when $\phi \rightarrow \phi + \pi$. In non-axial magnetic field (green arrows) this leads to the formation of $\hat{\mathbf{d}}$ solitons connecting HQVs pairwise (blue dash line). Vortex cores, vector $\hat{\mathbf{m}}$, nafen strands, and the axis of rotation are perpendicular to the plane of the picture.

II. VORTICES IN THE POLAR PHASE

The polar phase of superfluid ${}^3\text{He}$ is not stable as a bulk phase, but can be stabilized by confining it within nafen [25]. Nafen is a solid nanomaterial consisting of long parallel strands [29], Fig. 1. The polar phase order parameter can be expressed as

$$A_{\mu j} = \Delta_P \hat{\mathbf{d}}_{\mu} \hat{\mathbf{m}}_j e^{i\phi}. \quad (1)$$

Here Δ_P is the maximum gap in the quasiparticle energy spectrum, ϕ is the superfluid phase, and $\hat{\mathbf{d}}$ is a unit vector in the spin space. Vector $\hat{\mathbf{d}}$ is normal to the easy plane of magnetic anisotropy. Orbital anisotropy vector $\hat{\mathbf{m}}$ is locked along the nafen strands, while the node line in the energy spectrum develops in the plane perpendicular to the strands. Owing to the extension of the Anderson theorem [30–32], these features are robust against disorder, introduced by the nafen strands.

In our sample the strands (and thus vector $\hat{\mathbf{m}}$) are oriented along the axis of rotation. Thus, the superflow is applied in the plane perpendicular to the strands. In this plane the Landau critical velocity is zero, $v_{cL} = 0$.

The order parameter of the polar phase allows for both usual single-quantum phase vortices (SQV), around which $\phi \rightarrow \phi + 2\pi$, and half-quantum vortices (HQV), where $\phi \rightarrow \phi + \pi$ and $\alpha \rightarrow \alpha + \pi$ (see Fig. 2). Here α is the azimuthal angle of $\hat{\mathbf{d}}$ in the plane perpendicular to the magnetic field. The $\hat{\mathbf{d}}$ vector is kept in this plane by the Zeeman energy in the magnetic field of 11.2 mT applied in our experiments. Additionally pure spin vortices with winding $\alpha \rightarrow \alpha + 2\pi$ and $\phi = \text{const}$ around the core can exist, but they are not relevant for the critical velocity in applied mass flow, so we do not discuss them here.

We create an equilibrium array of HQVs by rotating the sample at the angular velocity Ω in zero (or axial)

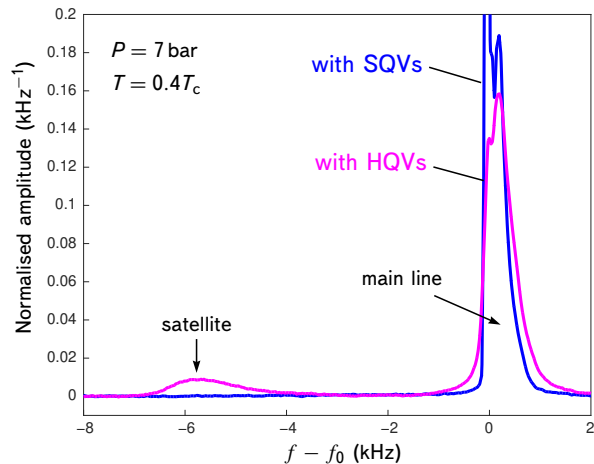


FIG. 3. Continuous-wave NMR spectra of the polar phase measured in the magnetic field transverse to nafen strands with HQVs and SQVs present in the sample. The horizontal axis shows the frequency shift from the Larmor value $f_0 = |\gamma|H/2\pi$, where γ is the gyromagnetic ratio of ^3He . The absorption normalized to the total spectrum area is plotted against the vertical axis. The HQVs produce a satellite in the NMR spectrum, while for SQVs no clear distinguishing features are seen. The states are produced as explained in Fig. 6 caption.

magnetic field while slowly cooling it down to the superfluid state [33]. If the magnetic field is applied transverse to the rotation axis and the nafen strands, HQVs become energetically unfavorable [34], and an array of SQVs is created on cooling through T_c .

III. OBSERVATION OF VORTICES WITH NMR AND MAGNON BEC

Observation of vortices in our measurements is based on nuclear magnetic resonance (NMR) techniques. All measurements are performed on the cubic sample with 4 mm edge filled with nafen with density 243 mg/cm^3 at the pressure 7 bar and temperature $0.4T_c$. Owing to spin-orbit interaction, $\hat{\mathbf{d}}$ solitons connecting HQVs pairwise present traps for standing spin waves in the transverse magnetic field. Those spin states are seen in the continuous-wave NMR spectrum as a satellite line with the negative frequency shift from the Larmor value, Fig. 3. The area of the satellite line I_{sat} is proportional to the total volume occupied by the solitons. In the equilibrium vortex state at the angular velocity Ω , the total number of vortices (and solitons) in the sample is proportional to Ω , the soliton length is the intervortex distance which is $\propto \Omega^{-1/2}$, and the soliton thickness $\sim 20 \mu\text{m}$ is fixed by the spin-orbit interaction. Thus, the total volume of all solitons and the satellite intensity $I_{\text{sat}} \propto \Omega^{1/2}$ [33].

On the other hand, SQVs cannot be easily identified based on cw NMR spectra, since SQVs are not associated

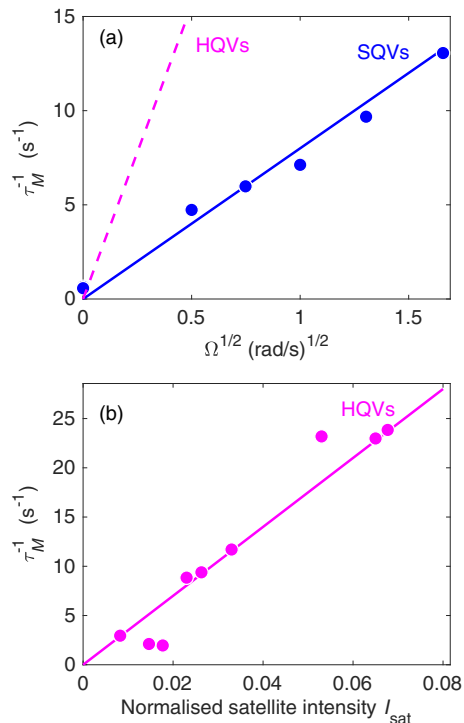


FIG. 4. Effect of vortices in the polar phase on the relaxation rate of the magnon BEC τ_M^{-1} . (a) The relaxation rate increases as a function of rotation velocity Ω applied at the transition to the superfluid state. For HQVs the shown slope is extracted from the data in Ref. [33] with the contribution of vortices, created by the Kibble-Zurek mechanism (KZM), removed. For SQVs the transition through T_c occurs in transverse magnetic field and thus KZM is suppressed by the symmetry-violating bias [35]. The measured points are shown by symbols and the line is a fit to $\Omega^{1/2}$ dependence. (b) As expected, for HQVs τ_M^{-1} (points) is proportional to the total volume of the $\hat{\mathbf{d}}$ -solitons between HQV cores, measured by the area of the satellite peak I_{sat} in the normalized NMR spectrum, like in Fig. 3. The line is a linear fit. For SQVs the origin of the magnon BEC relaxation remains unknown.

with a soliton structure and their cores are too small to provide noticeable contribution to the signal. We therefore use another detection technique, which is sensitive to both SQVs and HQVs. It is based on measuring the relaxation rate of a Bose-Einstein condensate of magnon quasiparticles. In superfluid ^3He magnons, pumped to the sample by a radio-frequency excitation pulse, are long-living excitations. Under appropriate conditions they form a quasiparticle Bose-Einstein condensate [27]. The condensation is manifested by coherent precession of the magnetization: In the whole condensate magnetization precesses with the same frequency and coherent phase, despite the inhomogeneity of the magnetic field or variations in the spin-orbit interaction strength. This coherent spin state was discovered in $^3\text{He-B}$ as Homogeneously Precessing Domain (HPD) [36] and has been recently observed also in the polar phase [28]. In $^3\text{He-B}$ such condensates were used as sensitive probes of temper-

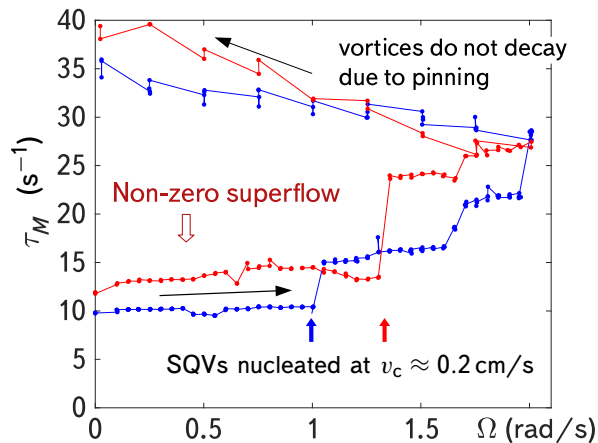


FIG. 5. Change of the magnon BEC relaxation τ_M^{-1} when the rotation velocity Ω is gradually increased from 0 to 2 rad/s and then decreased back to 0 at constant temperature, starting from the state with no vortices. Two traces for two independently prepared initial states are shown, the respective $\Omega(t)$ dependences are plotted in Fig. 6a. Single-quantum vortices form first at $\Omega \approx 1$ rad/s. Pinning prevents vortices from disappearance when Ω is decreased. Before vortex formation, stable superflow with velocity up to $v_c \approx 0.2$ cm/s exists in the sample, while the Landau critical velocity $v_{cL} = 0$ in the polar phase.

ature [37, 38], collective modes [39], spin supercurrents [40], analogue event horizon [41], and, most importantly in the context of this work, of vortices [42, 43].

By measuring the free induction decay signal after creating a magnon condensate by an excitation pulse in the transverse magnetic field, we have found that the relaxation rate is sensitive to vortices also in the polar phase, Fig. 4. Due to the inhomogeneity of our sample, the condensate splits at the end of its life time to several droplets in the minima of the effective potential. The relaxation rate τ_M^{-1} of the longest-living droplet is shown on the figures. From the signal amplitude, we estimate that the volume occupied by this droplet is about 2% of the total sample volume. Therefore, the magnon BEC in our case resembles more the so-called Q-balls [44–46], than the original HPD discovered in $^3\text{He-B}$.

In Fig. 4 the relaxation rate $\tau_M^{-1}(0) \approx 10 \text{ s}^{-1}$ measured in the absence of vortices is subtracted from the data. We attribute $\tau_M^{-1}(0)$ to the presence of the confining nafen matrix. For HQVs, τ_M^{-1} grows with the number of vortices and is proportional to the satellite intensity in the cw NMR spectrum, Fig. 4b. We conclude that the magnon BEC relaxation is concentrated in the $\hat{\mathbf{d}}$ solitons between HQVs, where the spin configuration deviates from the equilibrium.

When the sample contains SQVs, a clear increase of the magnon BEC relaxation is observed (Fig. 4a), while the satellite is absent (Fig. 3). For SQVs in $^3\text{He-B}$, the origin of the HPD relaxation is conversion of the magnons from the condensate to longitudinal spin waves (light Higgs quasiparticles) in the distorted orbital texture surround-

ing non-axisymmetric vortex cores [47]. In that case $\tau_M^{-1} \propto \Omega$ in the equilibrium vortex state. In the polar phase the structure of vortex cores is not known and expected to be substantially affected by the nafen strands with diameter ~ 0.1 of the core diameter and spaced by a few times larger distance. Simultaneously, the orbital texture is believed to be pinned by the strands. Thus, the origin of the magnon BEC relaxation from the single-quantum vortices in the polar phase (including its observed dependence $\tau_M^{-1} \propto \Omega^{1/2}$) remains unclear. That, however, does not prevent us from using τ_M^{-1} to observe the critical velocity related to the SQV creation and further evolution of the SQV density when Ω changes.

IV. MEASUREMENT OF THE CRITICAL VELOCITY FOR VORTEX FORMATION

We prepare the initial state for the critical velocity measurements by slowly cooling down the stationary sample through the superfluid transition in a transverse magnetic field. This procedure suppresses the formation of both HQVs and SQVs [35]. Then, at constant temperature, we gradually increase the rotation velocity in small steps, reducing the applied field to zero before changing the velocity. When the change is finished, we restore the transverse field and measure a few magnon BEC relaxation traces. The results are presented in Fig. 5.

There is a clear critical velocity, after which the relaxation rapidly grows, which we interpret as formation of quantized vortices. These vortices are seen to stay in the sample even when Ω is returned back to zero, as expected due to pinning on the nafen strands. After the Ω cycle is finished, we measure the cw NMR spectrum (blue line in Fig. 3 corresponds to the blue trace in Fig. 5) and find no satellite characteristic for half-quantum vortices. We thus infer that vortices formed during Ω cycle are SQVs. This means that in our experimental conditions the critical velocity for SQV formation is lower than that for forming HQVs. This is the case although the energy of an HQV pair is smaller than that of a single SQV in zero magnetic field (which is applied when Ω changes). A similar situation is observed in $^3\text{He-A}$, where the critical velocity for the double-quantum vortex skyrmions [48] is lower than that of SQVs, while the energy preference is the opposite [49].

Before first vortices are formed, the superfluid is in stable flow with non-zero velocity with respect to the walls of the container and to nafen strands, despite the fact that Landau critical velocity is zero in the polar phase. This supports the suggestion that super-Landau flow can be stable in fermionic superfluids owing to the formation of Bogoliubov Fermi surfaces. In our cubic container the flow is non-uniform and at $\Omega = 1$ rad/s the maximum flow velocity of 0.2 cm/s is reached in the middle of each side wall of the square container cross-section. This value is somewhat lower than $v_c \approx 1$ cm/s observed for SQVs in bulk $^3\text{He-B}$, where it was also found to depend strongly

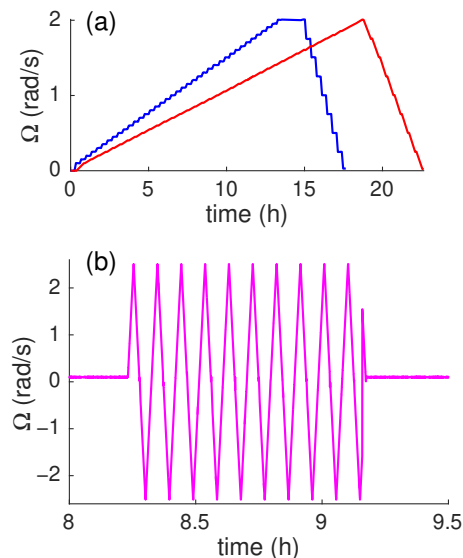


FIG. 6. Time dependence of rotation velocity $\Omega(t)$ for measurements of the critical velocity for vortex formations. (a) Slow changes in rotation velocity, corresponding to traces in Fig. 5 with the same colors, result in creation of SQVs only. The cw NMR spectrum measured at the end of the run marked with blue color is shown in Fig. 3 with the same color. (b) Rapid changes in rotation velocity over 24 hours do produce HQVs in addition to SQVs. One out of the ten periods of such drive applied in the course of the measurement in zero magnetic field is shown, corresponding to 1 cm/s maximum change in the flow rate in the sample container. The cw NMR spectrum measured after the run is shown in Fig. 3 with magenta color.

on the surface conditions [50]. For confined samples control of the surface conditions, especially at the boundaries of the confining matrix, remains a challenge for the future.

It is interesting that the magnon BEC relaxation observed at the maximum angular velocity during Ω sweep measurements in Fig. 5 exceeds that measured for equilibrium SQV array in Fig. 4a. We believe that due to nonuniform flow and pinning, the vortex array created with Ω sweep is also not uniform (see Section VI). Since the magnon BEC droplet measures vortex density locally, it is possible that a nonuniform vortex array can produce a larger signal than the equilibrium vortex distribution at the same Ω .

Remarkably, we are able to create also HQVs in the superfluid state by changing the rotation velocity rapidly enough. In this case SQV creation and annihilation is not able to compensate for changes in the rotation velocity fast enough, and local flow velocity can exceed the HQV critical velocity. We vary the rotation velocity between $\Omega = +2.25$ rad/s and -2.25 rad/s for several hours, see Fig. 6b. While the amount of SQVs created in this process increases magnon BEC relaxation beyond what can be measured, HQVs are also created, as seen from the appearance of the satellite in the cw NMR spectrum

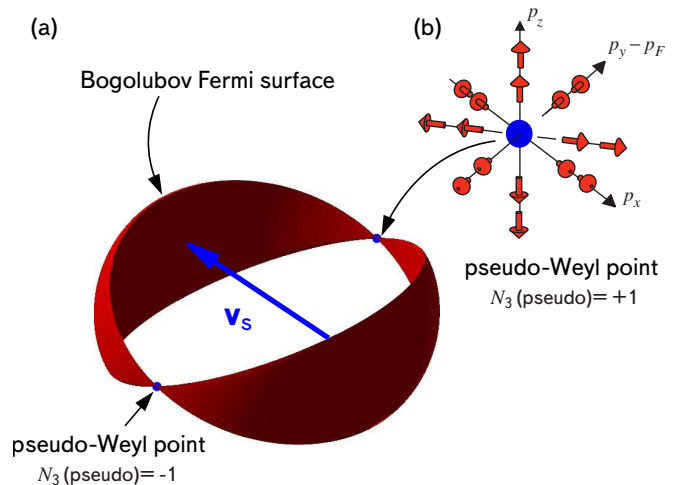


FIG. 7. Illustration of the Bogoliubov Fermi surface in polar phase in the presence of superflow \mathbf{v}_s . (a) BFS contains two Fermi pockets, which touch each other at two points. Here the superflow is applied along the x axis, and touching points are at $\mathbf{p} = \pm p_F \hat{\mathbf{y}}$. (b) The touching points are the pseudo-Weyl points. Their topology is illustrated as the hedgehog in momentum space, with the topological invariant in Eq. (5). Arrows show direction of the $\hat{\mathbf{n}}$ vector. For this figure the parameters in Eqs. (2) and (3) are chosen as $m^*c/p_F = 1/12$ and $v_s/c = 1/2$.

(magenta trace in Fig. 3). Therefore it is possible to set bounds for the HQV critical velocity for the conditions of the measurements: it exceeds 0.2 cm/s but is below 1 cm/s.

V. BOGOLIUBOV FERMI SURFACE IN THE POLAR PHASE

Detection of stable superflow in the polar phase is an indirect indication of the formation of the BFS. Let us discuss the structure and the topology of such Fermi surface and make predictions for observables, resulting from the appearance of the non-thermal normal component. Quasiparticle energy spectrum in presence of a superflow \mathbf{v}_s is Doppler shifted:

$$E(\mathbf{p}) = \epsilon(\mathbf{p}) + \mathbf{p} \cdot \mathbf{v}_s, \quad (2)$$

$$\epsilon^2(\mathbf{p}) = c^2 p_z^2 + v_F^2 (p - p_F)^2, \quad (3)$$

where v_F is Fermi velocity, and $c = \Delta_P/p_F$. The Bogoliubov Fermi surface is given by solution of the equation $E(\mathbf{p}) = 0$. Fig. 7 demonstrates the BFS for the superflow in the (x, y) plane transverse to the $\hat{\mathbf{m}}$ vector. Such Fermi surface resembles that in graphite, where the chain of touching electron and hole pockets is present [51–55].

The BFS in the polar phase has nontrivial topology associated with the conical touching points of the Fermi surface pockets at $\mathbf{p} = \pm p_F \hat{\mathbf{v}}_s \times \hat{\mathbf{z}}$. It is similar but not

identical to that of the Weyl point in Weyl semimetals and in $^3\text{He-A}$, as shown below. We thus call the touching points pseudo-Weyl points [55].

The Bogoliubov-de Gennes Hamiltonian for the polar phase can be written in terms of the vector $\mathbf{n}(\mathbf{p})$:

$$H = \tau_1 n_1(\mathbf{p}) + n_2(\mathbf{p}) + \tau_3 n_3(\mathbf{p}), \quad (4)$$

where τ_1 and τ_3 are Pauli matrices in the Bogoliubov-Nambu particle-hole space, and as distinct from the Weyl Hamiltonian the matrix τ_2 is missing. The components of the vector field $\mathbf{n}(\mathbf{p})$ are $n_1(\mathbf{p}) = cp_z$, $n_2(\mathbf{p}) = \mathbf{p} \cdot \mathbf{v}_s$ and $n_3(\mathbf{p}) = v_F(p - p_F)$. One can write the invariant, which is similar to that for the Weyl points:

$$N_3(\text{pseudo}) = \frac{1}{8\pi} e_{ijk} \int_{S_2} dS^k \hat{\mathbf{n}} \cdot \left(\frac{\partial \hat{\mathbf{n}}}{\partial p_i} \times \frac{\partial \hat{\mathbf{n}}}{\partial p_j} \right), \quad (5)$$

where the unit vector $\hat{\mathbf{n}} = \mathbf{n}/|\mathbf{n}|$, and S_2 is the spherical surface around the touching point. The topological charges of the two pseudo-Weyl points are $N_3(\text{pseudo}) = \pm 1$.

The BFS in the polar phase results in a finite density of states (DoS):

$$N(0) = \int \frac{d^3p}{(2\pi)^3} \delta(E(\mathbf{p})) = N_F \frac{v_s}{c}, \quad (6)$$

where $N_F = p_F m^*/\pi^2$ is DoS in normal liquid ^3He . This gives the linear in v_s additional heat capacity C and the finite density of the normal component at $T = 0$:

$$\frac{C(T)}{C_F(T)} = \frac{v_s}{c}, \quad \frac{\rho_n}{\rho} = \frac{v_s m^*}{c m}, \quad (7)$$

where $C_F(T)$ is heat capacity of normal liquid, and $m^* = p_F/v_F$ is effective mass. For $w \sim 0.2$ cm/sec the additional DoS is on the order of $0.05N_F$, which, in principle, should be detectable in heat capacity measurements.

The superflow also suppresses the gap amplitude. According to Muzikar and Rainer [56] the suppression of the gap at $T = 0$ and $v_s/c \ll 1$ is:

$$\Delta_P(v_s) = \Delta_P(0) \left(1 - \frac{v_s^3}{3c^3} \right), \quad v_s \ll c. \quad (8)$$

This modifies the spin-orbit interaction:

$$F_D = g_D (\hat{\mathbf{d}} \cdot \hat{\mathbf{m}})^2, \quad \frac{\delta g_D}{g_D} = -\frac{2v_s^3}{3c^3}. \quad (9)$$

A well-established method to measure the strength of the spin-orbit interaction in superfluid ^3He is through the shifts of the characteristic lines in the NMR spectra. The smallness of the expected effect in Eqs. (8) and (9) will, however, make this measurement challenging.

At finite temperature T relevant to experiments, the gap suppression is modified [57]:

$$\frac{\Delta(v_s, T)}{\Delta(0, 0)} = \left[1 - \alpha'_1 \frac{v_s^3}{c^3} - \alpha'_2 \frac{T^2 v_s}{T_c^2 c} \right], \quad T/T_c \ll v_s/c \ll 1 \quad (10)$$

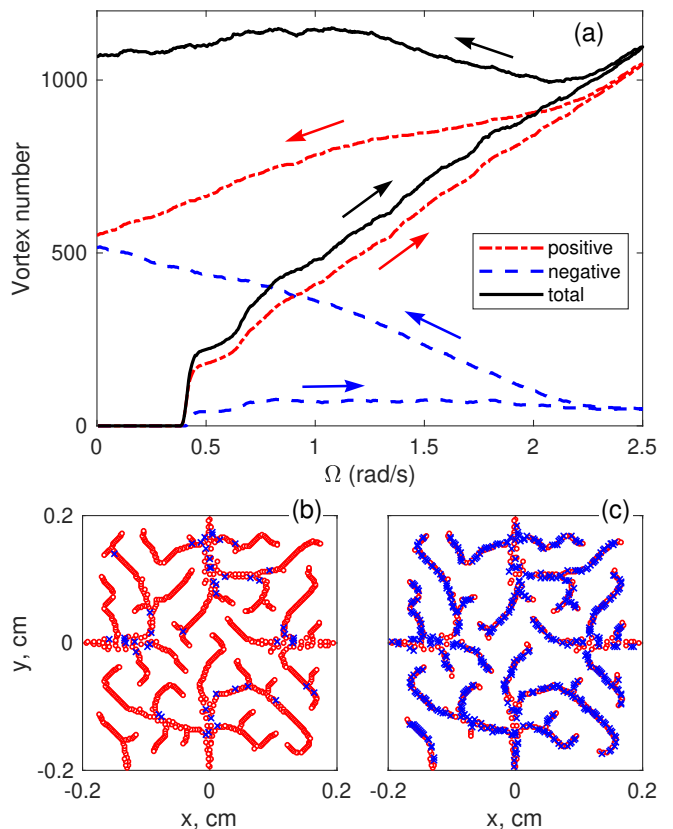


FIG. 8. Simulation of the vortex formation with pinning: (a) Number of vortices (red dash dot line), antivortices (blue dash line) and the sum of the two populations (solid black line), as a function rotation velocity Ω which is changed from 0 to 2.5 rad/s and back. (b) The configuration of vortices (red circles) and antivortices (blue crosses) at $\Omega = 2.5$ rad/s. (c) The final vortex configuration at $\Omega = 0$.

$$\frac{\Delta(v_s, T)}{\Delta(0, 0)} = \left[1 - \alpha_1 \frac{T^3}{T_c^3} - \alpha_2 \frac{v_s^2 T}{c^2 T_c} \right], \quad v_s/c \ll T/T_c \ll 1. \quad (11)$$

Here the parameters $\alpha_1, \alpha'_1, \alpha_2, \alpha'_2$ are of order of unity.

VI. NUMERICAL SIMULATIONS

We can gain qualitative understanding of the process that creates vortices during Ω sweep in the superfluid state with a simple numerical model (Fig. 8). In the simulation we study the cross section of a square sample container, rotated along the axis perpendicular to the cross section. The flow velocity is calculated as the sum of the potential flow in a box, and the contribution from vortices, which in the two-dimensional simulation are points. Vortices carry one quantum of circulation either in the positive direction (along rotation velocity) or in the opposite direction (antivortices).

We start from the configuration with no vortices and zero rotation velocity Ω . Then Ω is increased in small steps of $5 \cdot 10^{-3}$ rad/s. After each step we calculate the

superfluid velocity in the rotating frame on a grid of 201×201 points, which simulate pinning sites. If the flow velocity magnitude exceeds 0.1 cm/s (critical velocity in the simulation), a vortex or an antivortex is placed on the pinning site on the condition that the free energy of the system is lowered as a result. Vortices with positive and negative circulation at the same site annihilate each other. Once created, vortices are not allowed to move. This emulates the strong pinning by nafen observed experimentally [33]. The flow field of the vortex is then added to the total flow. Vortices can only be removed by the annihilation.

In this model, the resulting vortex configuration forms a non-uniform pattern (Fig. 8) which resembles that observed in superconducting thin-film systems where pinning is also strong [58–60]. The total number of vortices rapidly increases from zero when velocity of the potential flow exceeds the imposed critical velocity. This occurs at the middle of each of the four container walls. From those points avalanches of vortices emerge. This feature resembles the substantial jump in τ_M^{-1} at the critical velocity in the experiments. Thereafter vortex number in simulations grows more continuously.

When the rotation velocity is decreased, many of the vortices with positive circulation are annihilated by antivortices. The total number of vortex and antivortex points nevertheless mostly increases. Qualitatively these observations explain the features seen in the experiments. In particular, the simulation provides a scenario that explains why the observed magnon BEC relaxation rate never decreases with changes in the rotation velocity.

VII. CONCLUSIONS

In conclusion, we have experimentally observed stable superflow in the polar phase of ^3He at velocities exceeding the Landau critical velocity. The stability of superflow is limited by creation of single-quantum vortices (at velocities of about 0.2 cm/s) and half-quantum vortices (at velocities below 1 cm/s). This signifies formation of the Bogoliubov Fermi surface and of the non-thermal normal component at super-Landau velocities. The next exciting development will be to observe the contribution of the flow-induced quasiparticle states to thermodynamic quantities, e.g. those predicted by Eqs. (7), (8) and (11). In this respect the polar phase provides much brighter prospects than the ^3He -A phase, where

superflow exceeding the Landau limit was observed earlier: The polar phase possesses a whole node line, while the A phase has two point nodes. Hence, the contribution of the states below the Bogoliubov Fermi surface is expected to be significantly larger in the polar phase $\rho_n^{\text{polar}}(T=0)/\rho \sim p_F v_s / \Delta_P$ than in the A phase $\rho_n^{\text{A}}(T=0)/\rho \sim (p_F v_s / \Delta_A)^2$. Additional enhancement comes from the fact that the maximum $v_s \ll \Delta / p_F$, limited by vortex formation critical velocity is found to be larger in the polar phase, where vortices have hard cores, than in the A phase, where soft-core skyrmions are created.

We also find that vortex dynamics in our system is hindered by the strong pinning enforced by nafen, the nano-material used to stabilise the polar phase. In general, such vortex dynamics is closer to that in superconductors, than that in classical superfluids. We can generalize our results and conclude that appearance of protected zero-energy states in topological superfluids and superconductors does not prevent existence of stable superflow in such systems. While this stable state corresponds to the occupied Bogoliubov Fermi pockets, the initial process of filling the pockets during the super-Landau radiation of quasiparticles is also a fascinating problem for future research, as it has similarities to the Hawking radiation from the black-hole horizon [61–63]. Finally we note that recent successes in stabilization of uniform ultracold quantum gases [64] open possibilities to study superfluid dynamics in the regimes unaccessible in helium. It would be intriguing to observe evolution of the super-Landau superflow [65] in the crossover from the BCS to BEC regime via the unitary gas, when the spectrum of Bogoliubov excitations in the stationary system changes drastically.

ACKNOWLEDGMENTS

We thank V.V. Dmitriev for instructive discussions and providing the nafen sample. This work has been supported by the European Research Council (ERC) under the European Union’s Horizon 2020 research and innovation programme (Grant Agreement No. 694248). The experimental work was carried out in the Low Temperature Laboratory, which is part of the OtaNano research infrastructure of Aalto University. S. Autti acknowledges financial support from the Jenny and Antti Wihuri foundation.

-
- [1] P.W. Anderson and G. Toulouse, *Phase slippage without vortex cores: vortex textures in superfluid ^3He* , Phys. Rev. Lett. **38**, 508–511 (1977).
 [2] Onur Erten, Po-Yao Chang, Piers Coleman and Alexei M. Tsvelik, *Skyrme insulators: insulators at the brink of superconductivity*, Phys. Rev. Lett. **119**, 057603 (2017).
 [3] Ü. Parts, V.M.H. Ruutu, J.H. Koivuniemi, Yu. N.

- Bunkov, V.V. Dmitriev, M. Fogelström, M. Huenber, Y. Kondo, N.B. Kopnin, J.S. Korhonen, M. Krusius, O.V. Lounasmaa, P.I. Soininen, G.E. Volovik, *Single-vortex nucleation in rotating superfluid ^3He -B*, Europhys. Lett. **31**, 449–454 (1995).
 [4] G.E. Volovik, *The Universe in a Helium Droplet*, Clarendon Press, Oxford (2003).

- [5] G.E. Volovik, *Superconductivity with lines of GAP nodes: density of states in the vortex*, JETP Lett. **58**, 469 (1993).
- [6] K.A. Moler, D.J. Baar, J.S. Urbach, R. Liang, W.N. Hardy, and A. Kapitulnik, *Magnetic Field Dependence of the Density of States of $YBa_2Cu_3O_{6.95}$ as Determined from the Specific Heat*, Phys. Rev. Lett. **73**, 2744 (1994).
- [7] Y. Wang, B. Revaz, A. Erb, and A. Junod, *Direct observation and anisotropy of the contribution of gap nodes in the low-temperature specific heat of $YBa_2Cu_3O_7$* , Phys. Rev. B **63**, 094508 (2001).
- [8] G. R. Stewart, *Unconventional superconductivity*, Advances in Physics **66**, 75 (2017).
- [9] G.E. Volovik, *Zeros in energy gap in superconductors with high transition temperature*, Phys. Lett. A **142** 282–284 (1989).
- [10] W. V. Liu and F. Wilczek, *Interior Gap Superfluidity*, Phys. Rev. Lett. **90**, 047002 (2003).
- [11] D.F. Agterberg, P.M.R. Brydon, and C. Timm, *Bogoliubov Fermi surfaces in superconductors with broken time-reversal symmetry*, Phys. Rev. Lett. **118**, 127001 (2017).
- [12] N.F.Q. Yuan and Liang Fu, *Zeeman-induced gapless superconductivity with a partial Fermi surface*, Phys. Rev. B **97**, 115139 (2018).
- [13] P. M. R. Brydon, D. F. Agterberg, H. Menke, and C. Timm, *Bogoliubov Fermi surfaces: General theory, magnetic order, and topology*, Phys. Rev. B **98**, 224509 (2018).
- [14] S. Sumita, T. Nomoto, K. Shiozaki and Y. Yanase, *Classification of topological crystalline superconducting nodes on high-symmetry line: point nodes, line nodes, and Bogoliubov Fermi surfaces*, Phys. Rev. B **99**, 134513 (2019).
- [15] A.A. Zyuzin and P. Simon, *Disorder induced exceptional points and nodal lines in Dirac superconductors*, Phys. Rev. B **99**, 165145 (2019).
- [16] D.I. Bradley, S.N. Fisher, A.M. Guenault, R.P. Haley, C.R. Lawson, G.R. Pickett, R. Schanen, M. Skyba, V. Tsepelin, D.E. Zmeev, *Breaking the superfluid speed limit in a fermionic condensate*, Nature Phys. **12**, 1017–1021 (2016).
- [17] J. A. Kuorelahti, S. M. Laine and E. V. Thuneberg, *Models for supercritical motion in a superfluid Fermi liquid*, Phys. Rev. B **98**, 144512 (2018).
- [18] D. Vollhardt and P. Wölfle, *The superfluid phases of helium 3*, Taylor and Francis, London (1990).
- [19] T. Mizushima, Ya. Tsutsumi, T. Kawakami, M. Sato, M. Ichioka, K. Machida, *Symmetry protected topological superfluids and superconductors – From the basics to 3He* , J. Phys. Soc. Jpn. **85**, 022001 (2016).
- [20] L.V. Levitin, R.G. Bennett, A. Casey, B. Cowan, J. Saunders, D. Drung, Th. Schurig, J.M. Parpia, *Phase diagram of the topological superfluid 3He confined in a nanoscale slab geometry*, Science **340**, 841 (2013).
- [21] J.I.A. Li, J. Pollanen, A.M. Zimmerman, C.A. Collett, W.J. Gannon, W.P. Halperin, *The superfluid glass phase of 3He -A*, Nature Phys. **9**, 775 (2013).
- [22] L. V. Levitin, B. Yager, L. Sumner, B. Cowan, A. J. Casey, J. Saunders, N. Zhelev, R. G. Bennett, and J. M. Parpia, *Evidence for a Spatially Modulated Superfluid Phase of 3He under Confinement*, Phys. Rev. Lett. **122**, 085301 (2019).
- [23] A.J. Shook, V. Vadakkumbatt, P. Senarath Yapa, C. Doolin, R. Boyack, P.H. Kim, G.G. Popowich, F. Souris, H. Christani, J. Maciejko, and J.P. Davis, *Stabilized Pair Density Wave via Nanoscale Confinement of Superfluid 3He* , Phys. Rev. Lett. **124**, 015301 (2020).
- [24] K. Aoyama and R. Ikeda, *Pairing states of superfluid 3He in uniaxially anisotropic aerogel*, Phys. Rev. B **73**, 060504(R) (2006).
- [25] V. V. Dmitriev, A. A. Senin, A. A. Soldatov, and A. N. Yudin, *Polar Phase of Superfluid 3He in Anisotropic Aerogel*, Phys. Rev. Lett. **115**, 165304 (2015).
- [26] V.V. Dmitriev, A.A. Soldatov, and A.N. Yudin, *Effect of Magnetic Boundary Conditions on Superfluid 3He in Nematic Aerogel*, Phys. Rev. Lett. **120**, 075301 (2018).
- [27] Yu. M. Bunkov and G. E. Volovik, *Spin superfluidity and magnon BEC*, in *Novel Superfluids*, eds. K. H. Bennemann and J. B. Ketterson, International Series of Monographs on Physics **156**, 253 (2013).
- [28] S. Autti, V. V. Dmitriev, J. T. Mäkinen, J. Rysti, A. A. Soldatov, G. E. Volovik, A. N. Yudin, and V. B. Eltsov, *Bose-Einstein Condensation of Magnons and Spin Superfluidity in the Polar Phase of 3He* , Phys. Rev. Lett. **121**, 025303 (2018).
- [29] V. Dmitriev, L. Melnikovsky, A. Senin, A. Soldatov, and A. Yudin, *Anisotropic spin diffusion in liquid 3He confined in nafen*, JETP Lett. **101**, 808 (2015).
- [30] I. A. Fomin, *Analog of Anderson theorem for the polar phase of liquid 3He in nematic aerogel*, JETP **127**, 933 (2018).
- [31] V. B. Eltsov, T. Kamppinen, J. Rysti, and G. E. Volovik, *Topological nodal line in superfluid 3He and the Anderson theorem*, arXiv:1908.01645 (2019).
- [32] T. Hisamitsu, M. Tange, and R. Ikeda, *Impact of Strong Anisotropy on Phase Diagram of Superfluid 3He in Aerogels*, arXiv:1908.10712 (2019).
- [33] S. Autti, V. V. Dmitriev, J. T. Mäkinen, A. A. Soldatov, G. E. Volovik, A. N. Yudin, V. V. Zavjalov, and V. B. Eltsov, *Observation of Half-Quantum Vortices in Topological Superfluid 3He* , Phys. Rev. Lett. **117**, 255301 (2016).
- [34] N. Nagamura and R. Ikeda, *Stability of half-quantum vortices in equal-spin pairing states of 3He* , Phys. Rev. B **98**, 094524 (2018).
- [35] J. Rysti, S. Autti, G. Volovik, and V. Eltsov, *Kibble-Zurek creation of half-quantum vortices under symmetry violating bias*, arXiv:1906.11453 (2019).
- [36] A. S. Borovik-Romanov, Y. M. Bunkov, V. V. Dmitriev, and Y. M. Mukharskiy, *Long-lived induction signal in superfluid 3He -B*, JETP Lett. **40**, 1033 (1984).
- [37] S. N. Fisher, G. R. Pickett, P. Skyba, and N. Suramlishvili, *Decay of persistent precessing domains in 3He -B at very low temperatures*, Phys. Rev. B **86**, 024506 (2012).
- [38] P.J. Heikkinen, S. Autti, V.B. Eltsov, R.P. Haley, V.V. Zavjalov, *Microkelvin thermometry with Bose-Einstein condensates of magnons and applications to studies of the AB interface in superfluid 3He* , J. Low Temp. Phys. **175**, 681 (2014).
- [39] V.V. Zavjalov, S. Autti, V.B. Eltsov, P.J. Heikkinen, G.E. Volovik, *Light Higgs channel of the resonant decay of magnon condensate in superfluid 3He -B*, Nature Comm. **7**, 10294 (2016).
- [40] A. S. Borovik-Romanov, Y. M. Bunkov, V. V. Dmitriev, Y. M. Mukharskiy, and D. A. Sergatskov, *Investigation of spin supercurrents in 3He -B*, Phys. Rev. Lett. **62**, 1631 (1989).
- [41] M. Človečko, E. Gažo, M. Kupka, and P. Skyba, *Magnonic Analog of Black- and White-Hole Horizons in*

- Superfluid $^3\text{He-B}$* , Phys. Rev. Lett. **123**, 161302 (2019).
- [42] Y. Kondo, J. S. Korhonen, M. Krusius, V. V. Dmitriev, Y. M. Mukharsky, E. B. Sonin, and G. E. Volovik, *Direct observation of the nonaxisymmetric vortex in superfluid $^3\text{He-B}$* , Phys. Rev. Lett. **67**, 81 (1991).
- [43] J.J. Hosio, V.B. Eltsov, P.J. Heikkinen, R. Hänninen, M. Krusius, V.S. L'vov, *Energy and angular momentum balance in wall-bounded quantum turbulence at very low temperatures*, Nature Comm. **4**, 473 (2013).
- [44] Yu. M. Bunkov and G. E. Volovik, *Magnon Condensation into a Q Ball in $^3\text{He-B}$* , Phys. Rev. Lett. **98**, 265302 (2007).
- [45] S. Autti, Yu.M. Bunkov, V.B. Eltsov, P.J. Heikkinen, J.J. Hosio, P. Hunger, M. Krusius, and G.E. Volovik, *Self-Trapping of Magnon Bose-Einstein Condensates in the Ground State and on Excited Levels: From Harmonic to Box Confinement*, Phys. Rev. Lett. **108**, 145303 (2012).
- [46] S. Autti, P.J. Heikkinen, G.E. Volovik, V.V. Zavjalov, and V.B. Eltsov, *Propagation of self-localized Q-ball solitons in the ^3He universe*, Phys. Rev. B **97**, 014518 (2018).
- [47] S. M. Laine, E. V. Thuneberg, *Spin wave radiation from vortices in $^3\text{He-B}$* , Phys. Rev. B **98**, 174516 (2018).
- [48] R. Blaauwgeers, V. B. Eltsov, M. Krusius, J. J. Ruohio, R. Schanen and G. E. Volovik, *Double-quantum vortex in superfluid $^3\text{He-A}$* , Nature **404**, 471 (2000).
- [49] Ü. Parts, V. V. Avilov, J. H. Koivuniemi, N. B. Kopnin, M. Krusius, J. J. Ruohio, and V. M. H. Ruutu, *Coexistence of single and double quantum vortex lines*, Phys. Rev. B **62**, 5865 (2000).
- [50] V. M. H. Ruutu, Ü. Parts, J. H. Koivuniemi, N. B. Kopnin, and M. Krusius, *Intrinsic and extrinsic mechanisms of vortex formation in superfluid $^3\text{He-B}$* , J. Low Temp. Phys. **107**, 93 (1997).
- [51] G.P. Mikitik and Yu.V. Sharlai, *Band-contact lines in the electron energy spectrum of graphite*, Phys. Rev. B **73**, 235112 (2006).
- [52] G.P. Mikitik and Yu.V. Sharlai, *The Berry phase in graphene and graphite multilayers*, Fizika Nizkikh Temperatur **34**, 1012 (2008), [Low Temp. Phys. **34**, 794 (2008)].
- [53] G.P. Mikitik and Yu.V. Sharlai, *Dirac points of electron energy spectrum, band-contact lines, and electron topological transitions of $3\frac{1}{2}$ kind in three-dimensional metals*, Phys. Rev. B **90**, 155122 (2014).
- [54] T.T. Heikkilä and G.E. Volovik, *Nexus and Dirac lines in topological materials*, New J. Phys. **17**, 093019 (2015).
- [55] G.E. Volovik, *Topological Lifshitz transitions*, Fizika Nizkikh Temperatur **43**, 57 (2017), [Low Temp. Phys. **43**, 47 (2017)].
- [56] P. Muzikar and D. Rainer, *Nonanalytic supercurrents in $^3\text{He-A}$* Phys. Rev. B **27**, 4243–4250 (1983).
- [57] S.K. Yip and J.A. Sauls, *Nonlinear Meissner effect in unconventional superconductors*, Phys. Rev. B **51**, 16 233 (1995).
- [58] T. H. Johansen, M. Baziljevich, D. V. Shantsev, P.E. Goa, Y. M. Galperin, W.N. Kang, H.J. Kim, E.M. Choi, M.-S. Kim, and S. I. Lee, *Dendritic magnetic instability in superconducting MgB_2 films*, Europhys. Lett., **59**, 599 (2002).
- [59] M. Menghini, R. J. Wijngaarden, A. V. Silhanek, S. Raedts, and V. V. Moshchalkov, *Dendritic flux penetration in Pb films with a periodic array of antidots*, Phys. Rev. B **71**, 104506 (2005).
- [60] V. K. Vlasko-Vlasov, F. Colauto, A. A. Buzdin, D. Carmo, A. M. H. Andrade, A. A. M. Oliveira, W. A. Ortiz, D. Rosenmann, and W.-K. Kwok, *Crossing fields in thin films of isotropic superconductors*, Phys. Rev. B **94**, 184502 (2016).
- [61] G.E. Volovik, *Black hole and Hawking radiation by type-II Weyl fermions*, JETP Lett. **104**, 645 (2016),
- [62] Y. Kedem, E. J. Bergholtz, and F. Wilczek, *Black and White Holes at Material Junctions*, arXiv:2001.02625 (2020).
- [63] Long Liang and T. Ojanen, *Curved spacetime theory of inhomogeneous Weyl materials*, Phys. Rev. Research **1**, 032006 (2019).
- [64] B. Mukherjee, Z. Yan, P. B. Patel, Z. Hadzibabic, T. Yefsah, J. Struck, and M. W. Zwierlein, *Homogeneous Atomic Fermi Gases*, Phys. Rev. Lett. **118**, 123401 (2017).
- [65] H. Yamamura and D. Yamamoto, *Collective Excitation and Stability of Flowing Gapless Fermi Superfluids*, J. Phys. Soc. Jpn. **84**, 0444003 (2015).